Carbohydrate Polymers 195 (2018) 89–98

Contents lists available at ScienceDirect

Carbohydrate Polymers

journal homepage: www.elsevier.com/locate/carbpol

Stress transfer and matrix-cohesive fracture mechanism in microfibrillated cellulose-gelatin nanocomposite films

Franck Quero[a,*], Cristina Padilla[b], Vanessa Campos[b], Jorge Luengo[c], Leonardo Caballero[d], Francisco Melo[d], Qiang Li[e], Stephen J. Eichhorn[e,1], Javier Enrione[b]

[a] Laboratorio de Nanocelulosa y Biomateriales, Departamento de Ingeniería Química, Biotecnología y Materiales, Facultad de Ciencias Físicas y Matemáticas, Universidad de Chile, Avenida Beauchef 851, Santiago, Chile
[b] Biopolymer Research and Engineering Lab (BiopREL), Escuela de Nutrición y Dietética, Universidad de los Andes, Chile
[c] Research & Development Center, CMPC Celulosa S.A., Avenida Julio Hemmelmann 670, Nacimiento, Chile
[d] Departamento de Física, Universidad de Santiago de Chile, Av. Ecuador 3493, Santiago, Chile
[e] College of Engineering, Mathematics and Physical Sciences, University of Exeter, North Park Road, EX4 4QF Exeter, UK

ARTICLE INFO

Keywords:
Microfibrillated cellulose
Gelatin
Nanocomposite
Interface
Stress transfer
Fracture mechanism

ABSTRACT

Microfibrillated cellulose (MFC) obtained from eucalyptus was embedded in gelatin from two sources; namely bovine and salmon gelatin. Raman spectroscopy revealed that stress is transferred more efficiently from bovine gelatin to the MFC when compared to salmon gelatin. Young's modulus, tensile strength, strain at failure and work of fracture of the nanocomposite films were improved by ~67, 131, 43 y 243% respectively when using salmon gelatin as matrix material instead of bovine gelatin. Imaging of the tensile fracture surface of the MFC-gelatin nanocomposites revealed that crack formation occurs predominantly within bovine and salmon gelatin matrices rather than within the MFC or at the MFC/gelatin interface. This suggests that the mechanical failure mechanism in these nanocomposite materials is predominantly governed by a matrix-cohesive fracture mechanism. Both strength and flexibility are desirable properties for composite coatings made from gelatin-based materials, and so the findings of this study could assist in their utilization in the food and pharmaceutical industry.

1. Introduction

Gelatin is a well-known protein material that is typically obtained from animal meat production byproducts such as skin, tendons, and bones to cite a few examples. This natural polymer is currently used as additive in the food industry as well as in the pharmaceutical industry (Gómez-Guillén et al., 2009; Karim and Bhat, 2008; Schrieber, 2007) and in biomedical applications due to its well know viscoelastic and biological properties (Jaipan, Nguyen, & Narayan, 2017; Kuijpers et al., 2000). Gelatin is commonly obtained from mammalian tissue (porcine and bovine) but due to recent social, cultural and more recently bio-safety considerations other sources of this hydrocolloid are currently being explored. Gelatin from low temperature water marine species shows desirable viscoelastic properties related its low molecular weight and specific amino acid composition (Gómez-Guillén et al., 2002; Haug, Draget, & Smidsrød, 2004). Gelatin obtained from low temperature water fish sources tends to have lower concentration of the amino acids proline and hydroxyproline, which are responsible for the so-called triple-helix configuration formation and stabilization upon cooling (Mitchell and Ledward, 1986; Piez and Gross, 1960; Veis, 1964).

A characteristic of gelatin that is currently preventing its use for a wider number of applications is its brittle nature (low strength and flexibility). This is a problem inhibiting its use, both in the dried state, in the form of films or aerogels, and in the wet state in the form of hydrogels. As a result, obtaining gelatin-based materials that are both strong and flexible is a research challenge. Indeed, mechanical properties of these materials are particularly relevant for applications in food coatings and encapsulating technologies as well as in scaffold fabrication for tissue engineering. Gelatin obtained from mammals is more particularly brittle, especially when the triple-helix configuration content is maximized (Bigi, Panzavolta, & Rubini, 2004). Therefore, it is worth considering other gelatin sources to obtain mechanically stronger and more flexible materials.

MFC (a form of nanocellulose) is well known for its high elastic modulus (Tanpichai et al., 2012) and tensile strength (Page and El-Hosseiny, 1983; Saito, Kuramae, Wohlert, Berglund, & Isogai, 2013)

* Corresponding author.
E-mail address: fquero@ing.uchile.cl (F. Quero).
[1] Present address: Bristol Composites Institute (ACCIS), University of Bristol, Queen's Building, University Walk, Bristol, BS8 1TR, United Kingdom.

https://doi.org/10.1016/j.carbpol.2018.04.059
Received 22 January 2018; Received in revised form 22 March 2018; Accepted 15 April 2018
Available online 21 April 2018
0144-8617/

and its reinforcement ability has been demonstrated for a range of polymer matrices (Kargarzadeh et al., 2017; Lee, Aitomäki, Berglund, Oksman, & Bismarck, 2014). The reinforcement ability of nanocellulose in polyvinyl alcohol (PVA) has been investigated and found to be relatively successful, probably due to the hydrophilic nature of PVA. The mechanical properties of PVA were found to be significantly improved upon the addition of 8 wt% of nanocellulose (Sarwar, Niazi, Jahan, Ahmad, & Hussain, 2018). Other recently published work has been focused on comparing organic polyvinyl alcohol (PVA) and inorganic silica (SiO_2) as matrices for nanocellulose (Poyraz, Tozluoğlu, Candan, Demir, 2017; Poyraz, Tozluoğlu, Candan, Demir, Yavuz, 2017; Poyraz et al., 2018). Better tensile properties were obtained when using PVA as an organic matrix when compared to inorganic SiO_2. In some of these works, the pulp sources were pretreated using cellulase and/or sodium borohydride ($NaBH_4$) to, respectively, reduce the energy necessary for fibrillation and improve the dispersion and obtain a uniform size distribution of the nanocellulose (Tozluoğlu, Poyraz, Candan, Yavuz, & Arslan, 2017). Other studies have been focused on using nanocellulose to mechanically reinforce gelatin of mammalian origin. This has been achieved by adding controlled amounts of NFC or cellulose nanocrystals (CNCs) from bacterial and plant origins. The use of cellulose nanocrystals (CNCs) obtained from bacterial cellulose was found to maximize the tensile strength, tensile modulus and stiffness of gelatin at a weight fraction of 4% (George and Siddaramaiah, 2012). A more recent work has demonstrated that relatively good stress transfer can be obtained between gelatin and bacterial cellulose nanofibers (Quero et al., 2015). Another study, however, suggested that MFC and CNCs from plant origin, used at weight fractions of up to 10%, do not significantly improve the tensile mechanical properties of gelatin (Echegaray et al., 2016; Mondragon, Peña-Rodriguez, González, Eceiza, & Arbelaiz, 2015). Both these studies suggested that low interfacial stress transfer might be present between the gelatin matrix and the MFC and CNCs due to a low level of interfacial adhesion. No direct evidence of this has however been provided to date (Echegaray et al., 2016; Mondragon et al., 2015). Scanning electron microscopy images from the fracture surfaces of these materials, suggested a relatively good wetting of both MFC and CNCs by the gelatin matrix (Mondragon et al., 2015). The latter would indicate a good interface since no gap was observed at the nanocellulose/gelatin interface. It was, however, not clear how these fracture surfaces were obtained, either from cold fracture or tensile fracture, making it difficult to relate the mechanical properties obtained to the surface fracture morphology. From these studies, it seems that failure within these nanocomposites does not occur at the interface and so it is possible that failure may be occurring within the gelatin matrix due to its brittle nature and so the failure in these materials might be governed by a matrix-cohesive fracture mechanism. The reasons why poor mechanical properties have to date been obtained for these materials has not been clearly identified and explained. A direct comparison of gelatin matrix materials focusing on evaluating the reinforcement ability of MFC has also not been previously reported.

The present work focuses on quantifying the interfacial stress transfer from gelatin to MFC obtained from a plant source. The technique used for this is Raman spectroscopy, which is used to probe the interfacial interaction between the materials. In addition, this work identifies the dominant fracture mechanism that occurs in this form of nanocomposite, using two sources of gelatin; namely bovine gelatin and salmon gelatin.

2. Materials and methods

2.1. Materials and reagents

Bovine gelatin, with a Bloom of 200, was purchased from Rousselot (Brazil). All reagents were purchased as analytical grade from Merck (Germany) and Sigma Aldrich (USA) and were used as-received.

Salmon gelatin was extracted as follows. Salmon skins, donated by a local producer, were obtained from Atlantic salmon (*Salmo salar*) as described and characterized using methods as previously described (Díaz-Calderón et al., 2017). Firstly, the salmon skins were de-scaled, and any muscle was removed using a sharp knife. The cleaned skins were subsequently cut into ~2 cm^2 square pieces, which were submitted to chemical pre-treatment. They were first submerged into a solution of sodium hydroxide (1:6) at a concentration of 0.1 M while stirring using an overhead mechanical agitator at a constant speed at 10 °C for 1 h. The skins were then washed with distilled water.

The skins were then immersed into an aqueous solution of acetic acid, at a concentration of 0.05 M and then mechanically stirred at a temperature of 60 °C for 3.5 h. The pH was constantly monitored and adjusted to ~4 by adding controlled amounts of acetic acid whenever necessary. Upon completion of this extraction step, the pieces of skin were separated from the liquid supernatant using a metallic colander. The liquid supernatant was then filtered twice using a vacuum pump (Rocker 400, Rocker Scientific Co. Ltd, Taiwan) and paper filters having a retention of 22 µm (Grade 541, Whatman, United Kingdom) and finally dried at 55 °C for 48 h in Teflon-coated moulds in an oven (Wiseven, Korea). At the end of the drying process, films of salmon gelatin were obtained, which were converted into a fine powder using a knife mill (KN195 Knifetec, FOSS Analytical Co. Ltda., China). The salmon gelatin powder was stored hermetically at 5 °C until further use.

2.2. Preparation of microfibrillated cellulose

A never-dried commercial cellulose pulp (*eucalyptus* sp.) with an α-cellulose content of ~90% was used to obtain the MFC. Initially, the never-dried cellulose pulp concentration was adjusted to 10% w/w by adding controlled amounts of Milli-Q water. The cellulose suspension was then submitted to a refining process by using a PFI mill at 20,000 revolutions. The never-dried cellulose pulp was then further diluted at a concentration of 3% w/w, again by adding controlled amounts of Milli-Q water. The cellulose suspension was then submitted to a homogenization step using an Ultra-Turrax homogenizer (T-25 Digital Ultraturrax®, IKA, USA) for 5 min at 24,000 rpm. Finally, the cellulose suspension was submitted to 20 homogenization passes using a high-pressure homogenizer (GEA Niro Soavi PANDA Plus 2000) at a pressure of 800 bars. At the end of the process, a highly viscous MFC suspension was obtained having a solid content of ~2% w/w.

2.3. Preparation of microfibrillated-gelatin nanocomposites

~80 g of the MFC suspension (2% w/w) was added to a volume of distilled water of ~150 mL and subsequently agitated for 1 h using a magnetic stirrer at room temperature. The suspension was then sonicated for 30 min (6 cycles of 5 min applying cooling step in between) using an ultrasonic probe at a 160 W power (Branson Ultrasonic Sonifier™, S-250D, USA). ~10.5 g of gelatin powder (either bovine or salmon gelatin) was subsequently added to the aqueous NFC suspension, which was previously heated up to ~60 °C using a hot plate. The aqueous NFC-gelatin mixture was carefully agitated using a magnetic stirrer for 1 h at 60 °C to fully dissolve the gelatin powder into the aqueous MFC suspension. The MFC-gelatin suspension was then cooled down from 60 °C to 20 °C and the pH of the suspension was adjusted to a value of ~7 using sodium hydroxide and hydrochloride acid aqueous solutions having respective molarities of 2 M and 6 M. 40 mL of MFC-gelatin suspension was then slowly poured into polystyrene Petri dishes and allowed to dry under refrigeration conditions (5 °C) for at least 2 weeks in a temperature-controlled incubator (Velp Scientifica FOC215E, Italy). After complete water evaporation, the films were carefully peeled off the Petri dishes and exposed to silica gel in a desiccator and a constant weight was reached within ~1 month. The moisture content within the films was determined gravimetrically overnight at 105 °C and found to be ~7% by weight.

2.4. Characterization

2.4.1. Gelatin characterization

The molecular weight (M_w) distribution of bovine and salmon gelatin was determined by SDS-PAGE, using an 8% acrylamide gel and a 5% stacking gel. Samples were heated at 95 °C for 5 min before loading (67 µg of gelatin) and a standard molecular weight marker in the 10–250 kDa range was used (Kaleidoscope™, Precision Plus Protein Standards™, Biorad). The electrophoresis was run at 100 V and the resulting gel was stained with 0.25% Commassie blue R250.

Capillary viscometry was used to determine an average molecular weight for bovine and salmon gelatin. The dependence of the reduced viscosity (η_{red}) and inherent viscosity (η_{inh}) of a dilute polymer suspension on the concentration (c) is well established. At infinite dilution ($c \rightarrow 0$), η_{red} and η_{inh} are defined as the intrinsic viscosity [η] (Harding, 1997). The relation between $[\eta]$ and M_w can be determined with the following empirical Mark-Houwink Kuhn-Sakurada (MHKS) equation

$$[\eta] = K \cdot {M_w}^a \quad (1)$$

where K and an are constants that are dependent on the nature of the solvent and the polymer conformation (Harding, 1997). The determination of M_w of salmon (SG) and bovine gelatin (BG) was carried out using the values of a and K used by Veis (1964) using the following respective equations

$$[\eta]_{SG} = 8.6 \times 10^{-5} \cdot {M_w}^{0,74} \quad (2)$$

$$[\eta]_{BG} = 8.4 \times 10^{-6} \cdot {M_w}^{0,88} \quad (3).$$

Each gelatin suspension was prepared in 0.1 M NaCl at 5 concentrations ranging from 2 to 6 g/L and left overnight at 4 °C for complete hydration. The flow times of the gelatin suspensions at each concentration were measured with a Cannon-Fenske viscometer (size 50, Sigma Aldrich Z275271-1EA) immersed in a thermoregulated water bath at 50 °C. 7 mL aliquots of each suspension were placed in the viscometer and the flow time of each concentration was determined by measuring the time required for the suspension to flow from the top to the bottom mark of the viscometer. Each flow time was measured four times, and the experiment was performed twice for bovine and salmon gelatin. η_{red} and η_{inh} values were plotted against concentration, and the point of convergence between η_{red} and η_{inh} values was taken as the intrinsic viscosity [η].

The concentration of the amino acids glycine, proline and hydroxiproline in bovine and salmon gelatins was determined by reverse-phase high-performance liquid chromatography (HPLC-RP) as previously reported in the literature (Rebane and Herodes, 2010). Briefly, ~10 mg of sample was hydrolysed with a solution of 6 N HCl at 110 °C for 24 h. The obtained hydrolysate was derivatized with 20 mL of phenylthiocyanate (10% w/v) to generate phenylthiocarbamyl amino acids, and then separated and quantified by HPLC-RP at 254 nm. A liquid chromatograph (Waters 600 controller, Massachusets, USA) with a diode array detector (Waters 996) and a Phenomenex (Los Angeles, California, USA) Luna RP18 column (150 mm x 4.6 mm, particle size 5 mm) at 40 °C was used. Gradient separation was performed using 0.14 M anhydrous sodium acetate (pH 5.9)/acetonitrile (94:6 v/v) solution and HPLC-grade acetonitrile/water (60:40 v/v) solution. The injection volume was 20 mL and the running time was 30 min. Amino acid quantification was carried out using external standards of each analyzed amino acid (Sigma-Aldrich, Steinheim, Germany). The amino acid contents (glycine, proline and hydroxyproline) of bovine and salmon gelatin samples are reported as percentages (%) of the total present in the sample.

A rheometer (Discovery HR-2, TA Instruments) using a 5 cm diameter parallel plate (PLATE SST ST 5CM) with a 300-µm gap was used to carry out dynamic shear rheology measurements of bovine and salmon gelatin suspensions. Gelatin suspensions with a concentration of ~6.67% w/v was used for all measurements. The pH of these suspensions was adjusted to 7 using sodium hydroxide and hydrochloride acid aqueous solutions with molarity of 2 M and 6 M respectively before performing experiments. An oscillation temperature ramp program was applied and storage modulus (G′) and loss modulus (G″) curves were measured during a cooling ramp from 25 °C to 2 °C, with a ramp rate of 4 °C/min. After determination of the G' versus strain linear zone, a 10% deformation at a 1 Hz frequency was applied. The gelation temperature was determined using G′ and G″ curves crossovers during the cooling process. Each measurement was performed in triplicate and average and their associated standard deviations displayed as error bars are reported.

2.4.2. Microfibrillated cellulose characterization

Powder X-ray diffraction was used to reveal the crystalline structure and determine the crystallinity index of the MFC. Initially, films of microfibrillated cellulose having a thickness of ~80 µm were obtained by drying a MFC suspension in 90-mm-diameter polystyrene Petri dishe in an oven at 60 °C overnight. The MFC films were subsequently analyzed using an X-ray diffractometer (Phillips X'Pert Pro, UK) fitted with a CuK_α radiation source having a wavelength of 1.541 Å. The analyses were performed at a current of 30 mA and an acceleration voltage of 40 kV in the diffraction angle 2θ range of 5–35° using a step size of 0.02°.

The crystallinity index (χ_c) of the MFC was determined using two methods. The first method is referred to as the Integration Method (Park, Baker, Himmel, Parilla, & Johnson, 2010) and the equation

$$\chi_c = \frac{A_C}{A_C + A_A} \times 100 \quad (4)$$

was used to estimate the crystallinity index where A_c and A_a are the areas under the X-ray diffraction pattern corresponding respectively to the contribution of crystalline and amorphous regions. The second method is the Peak Height Method (Park et al., 2010; Segal, Creely, Martin, & Conrad, 1959)

$$\chi_c = \frac{I_{002} - I_{am}}{I_{002}} \times 100 \quad (5)$$

where I_{002} and I_{am} correspond respectively to the intensity of the (002) reflection plane and the intensity of the amorphous phase of cellulose ($2\theta = 18°$ for CuKα X-ray source). Experiments were performed in triplicate and averages and standard deviations from the mean are reported.

The morphology and the MFC diameter size distribution were assessed by atomic force microscopy (Nanoscope III, Veeco Co. Ltd., USA). An aqueous MFC suspension (2% w/w) was diluted to a concentration of 0.01% w/w by adding a controlled amount of Milli-Q water. This suspension was then sonicated for 30 min (6 cycles of 5 min with cooling step in between) using an ultrasonic probe (Branson Ultrasonic Sonifier™, S-250D, USA) at a power of 160 W, to reach a better dispersion of MFC within the Milli-Q water. Drops of the sonicated MFC suspension were deposited onto a mica substrate and dried in air under ambient conditions prior to imaging. Imaging of the dried MFC suspension drops, allowing the MFC' morphology to be viewed, was performed using silicon cantilevers in air tapping mode in the frequency range and a radius curvature of 264–339 kHz and 10–15 nm, respectively. The MFC diameter size distribution was estimated by performing more than 200 measurements of individual fibers from images having a low density of MFC for accurate diameter estimation using Nanoscope software.

2.4.3. Nanocomposite characterization

The crystalline structure of MFC-bovine gelatin and MFC-salmon gelatin nanocomposites was revealed by powder X-ray diffraction. Similar experimental conditions as mentioned in Section 2.4.2 were used. The thicknesses of the MFC-bovine gelatin and MFC-salmon gelatin nanocomposite films were respectively ~270 and ~240 µm.

Integration of the area under the diffraction peak located at a diffraction angle 2θ of ~8° was performed using OriginPro 8 SR0 V8.0724 (BT24, USA) to obtain values of integrated intensity. Experiments were performed in triplicate and average values and their associated standard deviations are reported.

The micromechanical interaction between the MFC and gelatin was quantified by using a Raman spectrometer (Renishaw RM-1000 system, UK). This spectrometer was coupled to an optical microscope (Leica, UK) equipped with a × 50 objective lens to focus the laser excitation source (near infrared, λ = 785 nm) on the samples' surface. The laser was used at its maximum power, which corresponds to a power of ~1 mW at the sample's surface (no surface burning was found to occur). Each Raman spectrum was obtained using an exposure time of 120 s as well as 3 accumulations in the Raman shift range of 1050–1150 cm^{-1}. The films that contained ~15% w/w of MFC were carefully cut into strips having dimensions of ~0.1 ± 0.01 mm in thickness, ~10 mm in width and ~25 mm in lengths. Each sample was subsequently inserted and secured between the fixed and mobile jaws of a miniaturized in-situ deformation rig (Deben Microtest, 200N load cell, UK) that was set in tensile mode. The displacement speed of the mobile clamp was set to 1 mm min^{-1}. The samples were then deformed, by applying extension steps of 0.02 mm until complete sample failure. At each extension increment, a Raman spectrum was recorded. For each spectrum, the exact position of the Raman initially located at ~1095 cm^{-1} was determined by fitting using a mixed Gauss/Lorentzian function and using an algorithm based on the work of Marquardt (Marquardt, 1963). The micromechanical interaction for MFC-bovine gelatin and for MFC-salmon gelatin nanocomposites was evaluated in triplicate. Average values of shift rate as a function of strain and stress and their respective standard deviations are reported. The stress values were calculated by dividing the force recorded at each extension increment of 0.02 mm by the respective cross section of each sample. The micromechanical interaction was quantified by fitting the detailed shifts towards a lower wavenumber as a function of strain and stress using a linear function. The gradient of fit of the linear function was used as a quantification of the micromechanical interaction or stress transfer between MFC and the gelatin matrices (bovine and salmon).

The tensile fracture surfaces of the samples (deformed up to complete failure during the tensile deformation tests) were imaged by using scanning electron microscopy (Hitachi S3200N SEM-EDS, Japan) and using an acceleration voltage of 15 kV. Prior to imaging, the samples were gold-coated for 2 min using a sputter coater. The atomic composition of the surface of single cellulose-containing fibers was identified by energy dispersive X-ray spectroscopy (Hitachi S3200N SEM-EDS, Japan).

3. Results and discussion

3.1. Gelatin characterization

Fig. 1 reports an image showing the typical molecular weight distribution for bovine and salmon gelatin as obtained by SDS-PAGE electrophoresis. The image shows that both gelatin sources display components with different molecular weights, with α-chains present as major constituents having molecular weights in the range of ~120 to 140 kDa. For bovine gelatin, the most representative and most well-defined bands correspond to positions of ~145 and ~130 kDa, which are associated with α_1-chains and α_2-chains respectively (Chiou et al., 2006; Díaz, López, Matiacevich, Osorio, & Enrione, 2011; Karim and Bhat, 2008; Schrieber, 2007; Zhang, Li, & Shi, 2006). For salmon gelatin, the most well-defined bands are observed at positions of ~130 and ~120 kDa, which are also associated with α_1-chains and α_2-chains respectively (Chiou et al., 2006; Díaz et al., 2011; Duan, Zhang, Liu, Cui, & Regenstein, 2018; Sinthusamran, Benjakul, & Kishimura, 2015). The presence of these bands has been previously reported for salmon gelatin and other cold- and warm-water fish gelatin, and have been associated with the presence of α-chains (Arnesen and Gildberg, 2007). Two other relatively strong bands can be seen at ~80 kDa for the salmon gelatin. These bands may arise due to the presence of lower molecular weight chains occurring due to hydrolytic effects that may occur under acidic extraction conditions (Díaz-Calderón et al., 2017).

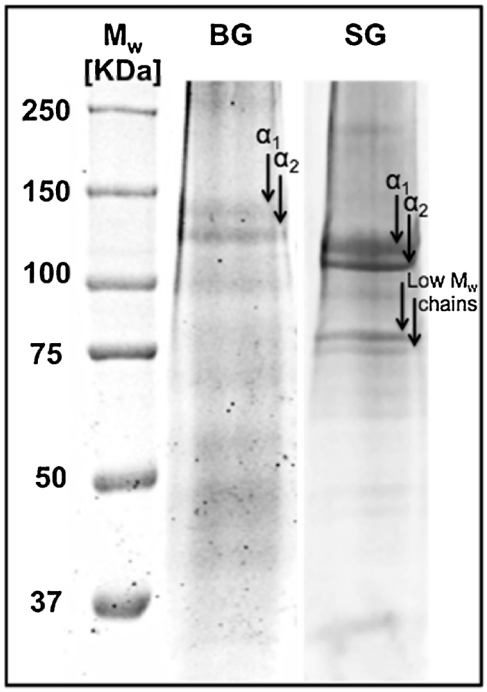

Fig. 1. A typical SDS-PAGE electrophoresis image of bovine gelatin (BG) and salmon gelatin (SG). The black arrows indicate the strongest bands that can be observed for bovine and salmon gelatin.

Fig. 2a and b report typical reduced and inherent viscosity data obtained for respectively bovine and salmon gelatins. From these data, the average molecular weight of bovine and salmon gelatin and were found to be respectively ~141 and ~86 kDa. These values are close to values previously reported in the literature and are within the range values of ~130–145 kDa and ~80–120 kDa obtained for bovine and salmon gelatin respectively, as determined by SDS-PAGE electrophoresis.

Fig. 3 reports typical G' and G" curves obtained from bovine and salmon gelatin suspensions. Fig. 3a compares typical G' curves obtained from bovine and salmon gelatin. One can see that upon cooling, the G' values for bovine gelatin suspension start increasing at a temperature of ~23 °C. This is due to the typical gelling property of bovine gelatin, which starts gelling at a relatively high temperature. This increase in the G' value occurs due to the formation of triple-helix configurations within the structure of gelatin suspensions. For salmon gelatin, the G' values start increasing at a much lower temperature; at ~8 °C. This difference between bovine and salmon gelatin may arise from their difference in average molecular weight but mainly due to differences in their respective amino acid compositions (Haug et al., 2004). Salmon gelatin has lower concentration of the amino acids proline and hydroxyproline (also sometimes referred to as imino acids) than bovine gelatin, as shown in Table 1. This result is consistent with previously reported results comparing the amino acid composition of cold-water, warm-water fish gelatin and mammalian gelatin (Chiou et al., 2006; Díaz et al., 2011; Gudmundsson, 2002). These amino acids have been reported to be responsible for the formation of triple-helix configurations and stabilization upon cooling (Berisio, Granata, Vitagliano, & Zagari, 2004; Gilsenan and Ross-Murphy, 2000; Mitchell and Ledward, 1986; Piez and Gross, 1960). The formation of these configurations

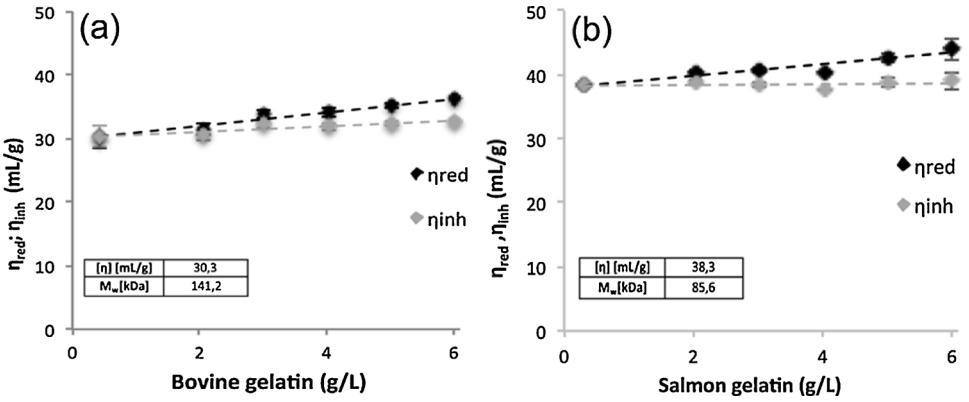

Fig. 2. Double extrapolation reduced viscosity (η_{red}) and inherent viscosity (η_{inh}) for the determination of the intrinsic viscosity [η] of (a) bovine and (b) salmon gelatin suspensions. Average molecular weight (M_w) and intrinsic viscosity are reported as insets for bovine and salmon gelatins.

explain why gelling of salmon gelatin suspensions occurs at a lower temperature than bovine gelatin in the present study, which is consistent with previous reports in the literature (Arnesen and Gildberg, 2007; Gudmundsson, 2002).

Fig. 3b and c report G' and G" values as a function of temperature for, respectively, bovine and salmon gelatin suspensions. For both gelatin sources, G' and G" values increase upon cooling and a cross-over point (as indicated by the black arrows in Fig. 3b and c) occurs between G' and G" curves at a temperature of 18.4 ± 0.1 °C and 5.1 ± 0.1 °C for bovine and salmon gelatin suspensions respectively. These values correspond to the gelling temperature of bovine and salmon gelatin suspensions. This result is consistent with results obtained before in the

Table 1
Glycine, proline and hydroxyproline contents in percentage (%) in bovine and salmon gelatin as measured by reverse-phase high-performance liquid chromatography.

Aminoacid	Percentage from total aminoacids in gelatin (%)	
	Bovine	Salmon
Glycine	24.79 ± 0.09	25.66 ± 0.04
Proline	11.75 ± 0.09	9.91 ± 0.07
Hydroxyproline	13.04 ± 0.01	8.26 ± 0.15

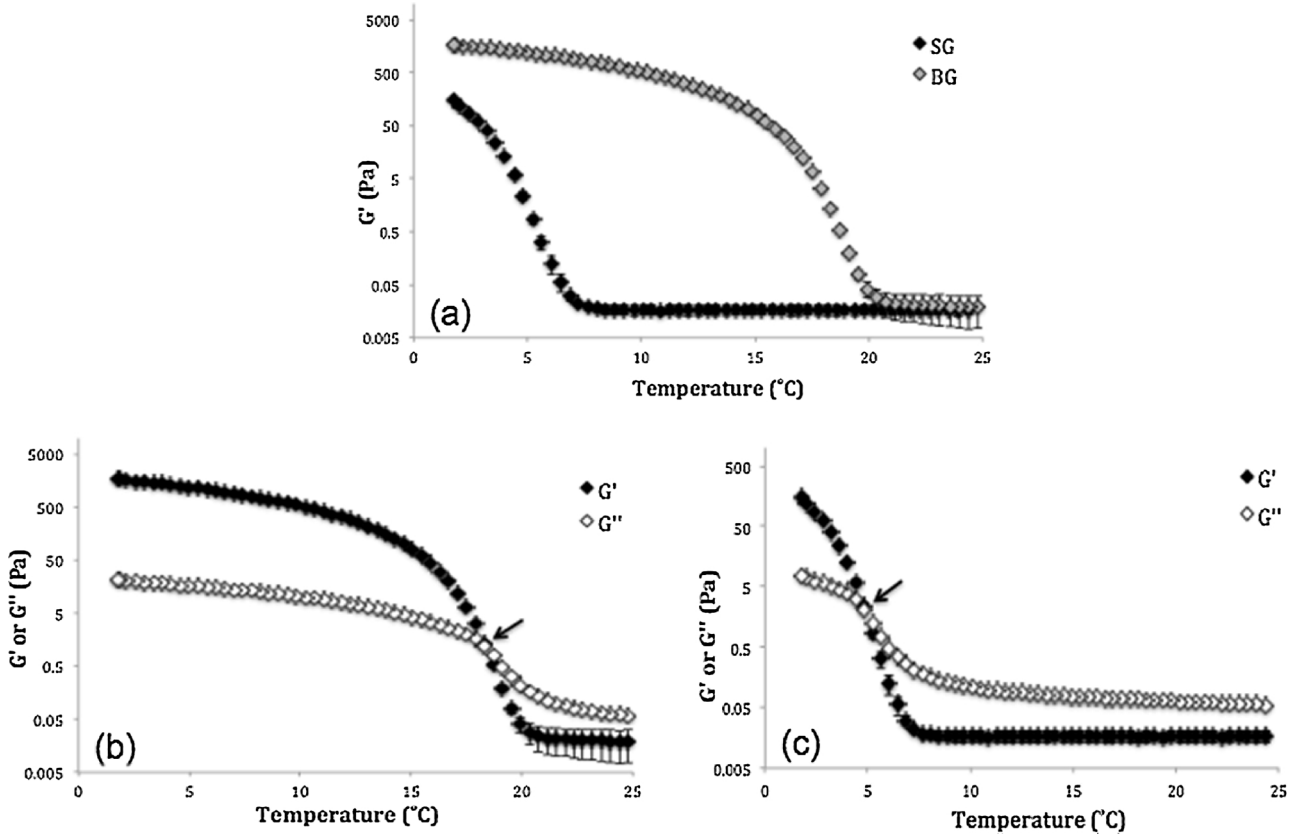

Fig. 3. (a) Storage modulus (G') variation of bovine (BG) and salmon gelatin (SG) suspensions during cooling. (b) Bovine gelatin gelation temperature determination through storage modulus (G') and loss modulus (G") variations during cooling. (c) Salmon gelatin gelation temperature determination through storage modulus (G') and loss modulus (G") variations as a function of temperature during cooling. Black arrows indicate the gelling temperatures of bovine and salmon gelatin. Error bars correspond to standard deviations from the mean and are sometimes smaller than symbols themselves.

literature where gelatin from cold-water fish was found to have a lower gelling temperature compared to warm-blooded animals, which behave differently to mammalian gelatin due to a difference in amino acids proline and hydroxyproline content (Gilsenan and Ross-Murphy, 2000; Gómez-Guillén et al., 2009; Gudmundsson, 2002; Haug et al., 2004).

3.2. Microfibrillated cellulose characterization

Supplementary data 1 reports a typical powder X-ray diffraction pattern for a film made of MFC. This pattern is typical for diffractograms reported for semi crystalline polymeric materials. A broad hump corresponding to amorphous material and relatively sharp peaks corresponding to crystalline material are clearly present. From this pattern, overlapping peaks positioned at diffraction angles 2θ of ~14.8 and 16.3° and another diffraction peak positioned at a diffraction angle 2θ of ~22.3° are observed. These three Bragg peaks have been reported before for MFC obtained from cellulose extracted from eucalyptus (which contains predominantly the cellulose Iα crystalline form). The peaks correspond respectively to the diffraction planes (101), (10$\bar{1}$), (002) (Besbes, Alila, & Boufi, 2011; Qing et al., 2013; Tonoli et al., 2012). From this pattern, the crystallinity index was estimated; values of 43 ± 3% and 69 ± 2% using the integration and peak height methods respectively were found. These values are within the range of ~40 to 80% typically reported in the literature for the crystallinity index of MFC obtained from mechanical fibrillation methods and determined by powder XRD using the peak height method (Abdul Khalil et al., 2014; Lavoratti, Scienza, & Zattera, 2016; Park et al., 2010; Qing et al., 2013). This method has been reported to overestimate values of crystallinity index compared to other methods, among them the integration method (French, 2014; Park et al., 2010; Qing et al., 2013). In the present study, the peak height method was used for literature comparison purposes only.

Fig. 4 reports AFM images obtained from low concentration MFC suspensions at various scales, ranging from 2 µm down to 250 nm (from Fig. 4a–e). From those images, one can observe the typical fiber-like morphology for MFC obtained after applying several high-pressure homogenization steps to a cellulose pulp. One can however observe that the diameter of these fibers varies from ~20 to 200 nm as shown in Fig. 4f where the fiber-diameter distribution is reported. These fibers can be classified as MFC due to their relatively wide distribution of widths. The appearance of these AFM images is similar to those reported previously in the literature for MFC (Benhamou, Kaddami, Magnin, Dufresne, & Ahmad, 2015).

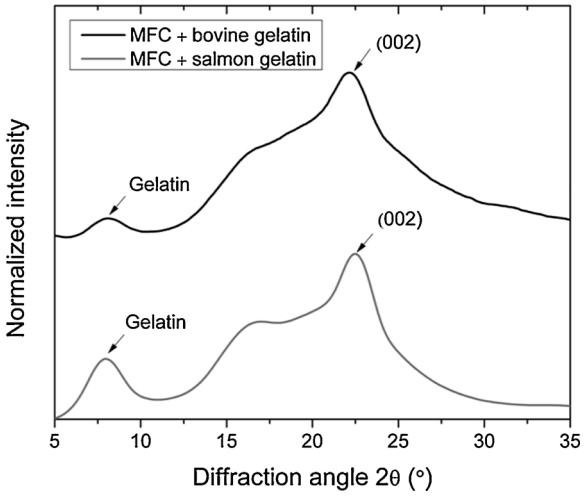

Fig. 5. Typical powder X-ray diffraction patterns for microfibrillated cellulose (MFC)-bovine gelatin and MFC-salmon gelatin nanocomposite films. Black arrows indicate the presence of diffraction peaks located at ~2θ = 8° and ~2θ = 22° corresponding respectively to the presence of triple-helix configurations present within the bovine and salmon gelatin matrices and to the (002) diffraction plane occurring from the crystalline phase of the MFC.

3.3. Nanocomposite characterization

Fig. 5 reports powder X-ray diffraction patterns from MFC-bovine gelatin and MFC-salmon gelatin nanocomposite films. Both patterns exhibit a Bragg peak at a diffraction angle 2θ of ~8°. The presence of this diffraction peak has been previously reported in the literature and has been attributed to the presence of triple-helix configurations that can form in gelatin upon cooling (Badii, MacNaughtan, Mitchell, & Farhat, 2014; Fadel, Hassan, & Oksman, 2012). The integrated intensity

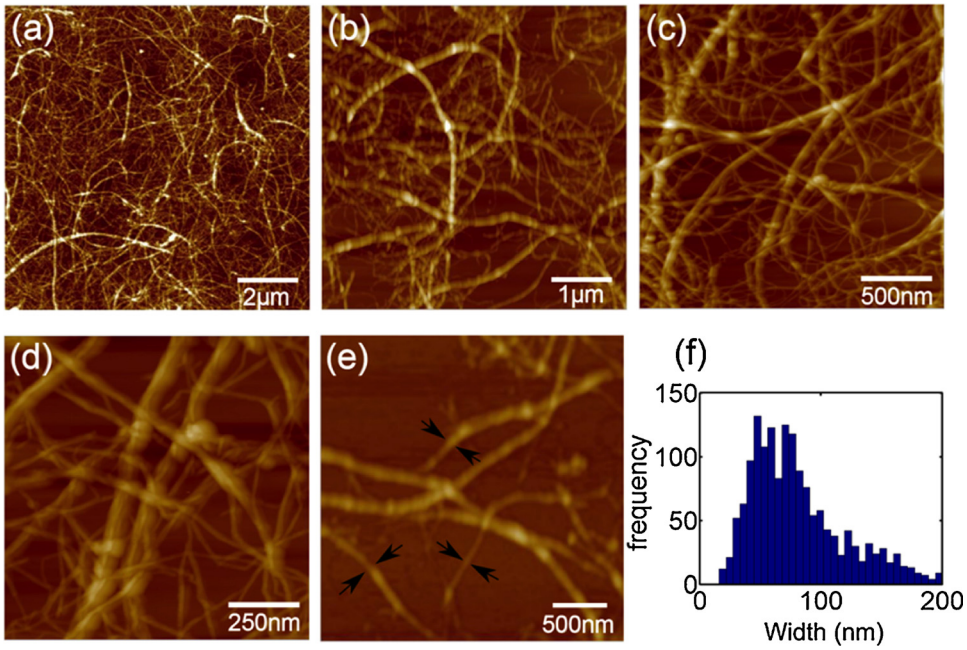

Fig. 4. Atomic force microscopy images obtained for microfibrillated cellulose (a-e) and a distribution of fiber width (f). In Fig. 4(e), a typical low-density region of microfibrillated cellulose is shown where black arrows indicate three specific fiber diameter estimations.

of that diffraction peak has been found to be proportional to the content of triple-helix configurations in gelatin and gelatin-based composites (Badii et al., 2014; Bigi et al., 2004; Yakimets et al., 2005). The integrated intensity values corresponding to the area under the peak located at a diffraction angle 2θ of ~8° were found to be 0.3 ± 0.1 and 1.0 ± 0.3 1/° for respectively MFC-bovine gelatin and MFC-salmon gelatin nanocomposite films. One can see that the integrated intensity of that diffraction peak for MFC-bovine gelatin nanocomposites is significantly lower than for MFC-salmon gelatin nanocomposites, suggesting that an increased amount of triple-helix configuration is present within the salmon gelatin matrix compared to the bovine gelatin matrix. This increased formation of triple-helix configurations might be due to the lower average molecular weight of salmon gelatin compared to bovine gelatin, which may favor molecular mobility during film formation.

In addition to the diffraction peak located at an angle 2θ of ~8°, both patterns exhibit a diffraction peak at an angle of ~22°. As shown in Supplementary data 1, this diffraction peak can be attributed to the presence of MFC in the bovine and salmon gelatin matrices. Similar patterns have been reported when bacterial cellulose is embedded in bovine gelatin (Quero et al., 2015).

Fig. 6a and b report Raman spectra for MFC-bovine gelatin and MFC-salmon gelatin nanocomposites in the Raman shift range of 1050–1150 cm^{-1}. One can observe the presence of a relatively well-defined Raman band located at a Raman shift of ~1095 cm^{-1}, which has been previously assigned to the vibrational motions of C—O and C—O—C moieties within the backbone molecular structure of cellulose (Gierlinger, Schwanninger, Reinecke, & Burgert, 2006; Wiley and Atalla, 1987). This band occurs due to the presence of MFC that have been embedded in the gelatin matrices. In previously reported work, it was shown that cellulose can be detected when embedded in a gelatin matrix, allowing the study of gelatin-cellulose interfaces (Quero et al., 2015). In this work, both materials were found to be spectroscopically distinct in the Raman shift range of 1050–1150 cm^{-1}.

As shown in Fig. 6a and b, the Raman band located at ~1095 cm^{-1} was found to shift towards a lower wavenumber, for MFC-bovine gelatin and MFC-salmon gelatin nanocomposites, upon the application of tensile deformation. This band has been reported before in the literature to shift towards a lower wavenumber upon the application of an external tensile deformation for a number of nanocellulose-containing composites (Bulota, Tanpichai, Hughes, & Eichhorn, 2012; Rusli and Eichhorn, 2008; Rusli, Shanmuganathan, Rowan, Weder, & Eichhorn, 2010; Tanpichai, Sampson, & Eichhorn, 2014) and also for a form of bacterial cellulose-gelatin composite (Quero et al., 2015). These shifts towards a lower wavenumber demonstrate that stress transfer is occurring from both gelatin sources (bovine and salmon) to the MFC in both nanocomposite materials.

Fig. 7a and b report detailed shifts towards a lower wavenumber for the Raman band initially located at ~1095 cm^{-1} as a function of strain and stress respectively, both for MFC-bovine gelatin and MFC-salmon gelatin nanocomposites. A linear shift that has been previously reported for a number of nanocellulose-containing composites (Bulota et al., 2012; Rusli and Eichhorn, 2008; Rusli et al., 2010; Tanpichai et al., 2014). In Fig. 7a, where these shifts are reported as a function of strain, no significant difference between the gradient of fit to shift data for MFC-bovine gelatin and MFC-salmon gelatin nanocomposites is observed. Average values and their standard deviations of $-0.25 \pm 0.05\ cm^{-1}\%^{-1}$ and $-0.28 \pm 0.02\ cm^{-1}\%^{-1}$ were obtained for MFC-bovine gelatin and MFC-salmon gelatin nanocomposites respectively. These values are close to values reported in the literature for MFC networks and composites (Bulota et al., 2012; Tanpichai et al., 2014) but lower than the initial average value of $-0.63 \pm 0.2\ cm^{-1}\%^{-1}$ recently reported for bacterial cellulose-gelatin composites (Quero et al., 2015). In Fig. 7b, where the detailed shifts are reported as a function of stress, one can observe a significant difference between the gradient of fit to data for MFC-bovine gelatin and MFC-salmon gelatin nanocomposites. Average values of $-27 \pm 3\ cm^{-1}\ GPa^{-1}$ and $-18 \pm 2\ cm^{-1}\ GPa^{-1}$ were found respectively. This difference in these shift values suggests that stress is more efficiently transferred from bovine gelatin to the MFC compared to salmon gelatin. This may arise because bovine gelatin has a higher content of proline and hydroxyproline amino acids compared to salmon gelatin, especially in hydroxyproline as reported in Table 1. These amino acids have been reported to be the most distinctive amino acids present in gelatin when comparing cold fish gelatin with warm fish and mammalian gelatin sources (Arnesen and Gildberg, 2007; Chiou et al., 2006; Díaz et al., 2011; Gilsenan and Ross-Murphy, 2000; Gómez-Guillén et al., 2009; Gudmundsson, 2002). Hydroxyproline has been reported to be a polar amino acid (Pei et al., 2013), which may favor the interaction of gelatin (through the presence of polar hydroxyproline) with the polar hydroxyl groups of cellulose present at the MFC surface. Proline, however, has been reported to be non-polar (Pei et al., 2013). If a high amount of hydroxyproline is present in the gelatin source (*c.f.* bovine gelatin), a relatively strong interface with MFC might be expected due to the formation of a relatively high level of non-bond interactions such as hydrogen bonding. In addition to the presence of strong hydrogen bonding, hydrophobic interactions may also occur. These interactions have been reported to be the primary driving force of binding between cellulose and aromatic rings of amino acids (Liu et al., 2011). Hydroxyproline and proline amino acids do not, however, possess any aromatic ring in their molecular structure. Since salmon gelatin contains less proline and hydroxyproline than bovine gelatin, the formation of a relatively soft interface could be expected due to the formation of fewer hydrogen bonding interactions. A question remains as to whether an improved stress transfer or strong interface might be beneficial for the mechanical properties of these gelatin-matrix nanocomposite materials. Interestingly, the shift rate with respect to stress, obtained in the present work for MFC-bovine gelatin nanocomposites, is similar to a value of $-27 \pm 3\ cm^{-1}\ GPa^{-1}$ reported recently for bacterial cellulose-bovine gelatin composites (Quero et al., 2015). However, in the previous work the cellulose weight content was 10% w/w and not 15% w/w like in the present study. If one

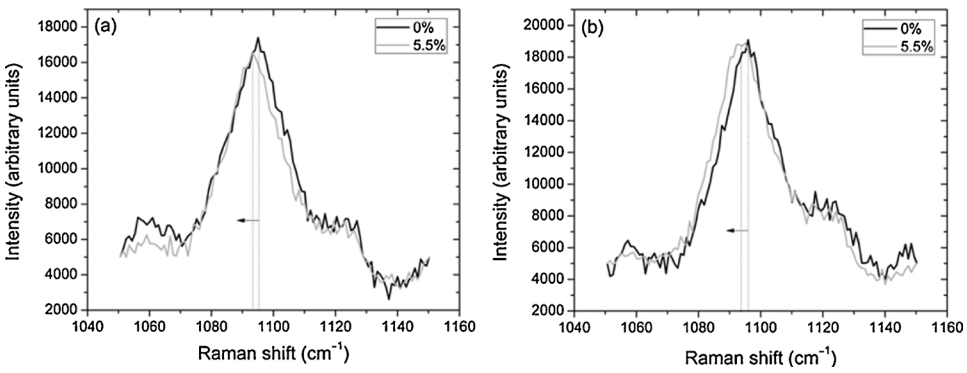

Fig. 6. Typical shifts in the Raman band initially located at ~1095 cm^{-1} towards a lower wavenumber for (a) microfibrillated cellulose-bovine gelatin and (b) microfibrillated cellulose-salmon gelatin nanocomposite films upon the application of external tensile deformation (5.5% strain). Black arrows indicate the typical shifts towards a lower wavenumber for the Raman band initially located at ~1095 cm^{-1}.

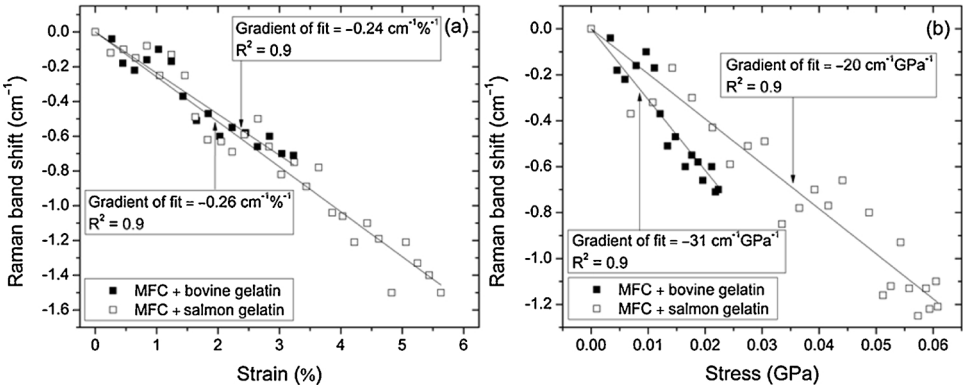

Fig. 7. Typical detailed shifts in the position of a Raman band initially located at ~1095 cm^{-1} towards a lower wavenumber for microfibrillated cellulose (MFC)-bovine gelatin and microfibrillated cellulose-salmon gelatin nanocomposite films, as a function of (a) strain and (b) stress.

normalizes these values with respect to the cellulose weight content, values of 2.7 and 1.8 $cm^{-1}\,GPa^{-1}\%^{-1}$ for bacterial cellulose-gelatin and MFC-gelatin composites are respectively obtained. This suggests that stress is potentially more efficiently transferred from bovine gelatin to bacterial cellulose compared to MFC. This result is consistent with the fact that stress transfer is usually more efficiently transferred from polymer matrices to bacterial cellulose (Quero et al., 2015; Quero et al., 2012; Quero et al., 2010) compared to when MFC are used (Bulota et al., 2012; Tanpichai et al., 2014). One reason for this might be due to the fact that stress is intrinsically more efficiently transferred within bacterial cellulose networks compared to MFC networks due to the interconnected nanofiber network of the former (Tanpichai et al., 2012).

Fig. 8 reports typical stress-strain curves for MFC-bovine gelatin and MFC-salmon gelatin nanocomposites. The detailed mechanical properties for these materials are reported in Supplementary data 2. From these data, one can see that Young's modulus, stress and strain at failure as well as the work of fracture are significantly higher for MFC-salmon gelatin nanocomposites compared to MFC-bovine gelatin nanocomposites at a MFC fraction of 15% w/w. This shows that these salmon gelatin-based nanocomposite materials have better mechanical performance (both strength and flexibility are improved) compared to bovine gelatin-based nanocomposite materials, despite the fact that it was previously demonstrated using Raman spectroscopy that stress transfer is better transferred from the bovine gelatin matrix to the MFC compared when a salmon gelatin matrix is used. The high content of triple-helix configurations present in the MFC-salmon gelatin nanocomposites

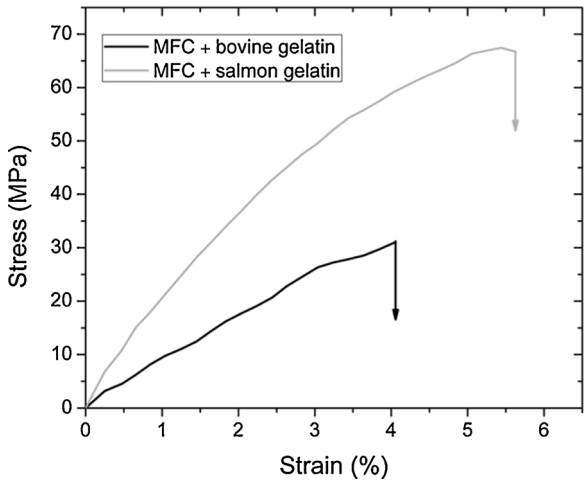

Fig. 8. Typical stress-strain curves for microfibrillated cellulose (MFC)-bovine gelatin and microfibrillated cellulose-salmon gelatin nanocomposite films. Arrows pointing downwards indicate complete sample failure.

compared to the MFC-bovine gelatin nanocomposites, as reported in Fig. 5, may also contribute to the improved mechanical performance of the MFC-salmon gelatin nanocomposites compared to the MFC-bovine gelatin nanocomposites. These triple helix configurations represent crystalline structures that can act as mechanical reinforcement in these gelatin-matrix nanocomposites (Bigi et al., 2004). The higher work of fracture and less brittle behavior measured for MFC-salmon gelatin nanocomposites compared to MFC-bovine gelatin nanocomposites might be attributed to the higher molecular mobility of the amorphous fraction of salmon gelatin compared to the amorphous fraction of bovine gelatin. This has been previously attributed to the lower glass transition temperature of salmon gelatin films compared to bovine gelatin (Díaz et al., 2011; Matiacevich, Celis Cofré, Schebor, & Enrione, 2013). This higher molecular mobility may be due to the lower average molecular weight and viscosity of salmon gelatin compared to bovine gelatin as reported respectively in Figs. 2 and 3.

Fig. 9a and b report typical scanning electron microscopy images obtained from the tensile fracture surfaces of MFC-bovine gelatin and MFC-salmon gelatin nanocomposites. The presence of MFC are noted, surrounded by the gelatin matrix (cf. respective arrows on the images). For both materials, the interface between the MFC and the gelatin is intact. No gap is observed between the MFC and the gelatin matrix. This result has been previously reported for MFC-gelatin nanocomposites (Mondragon et al., 2015) and is expected since both cellulose and gelatin are hydrophilic materials and from their molecular composition, one could expect a good interaction between these materials. When areas corresponding to the gelatin matrix are observed more closely, the presence of a high number of nanosized cracks is noted. Given this fact, and that there is a relatively intact interface between the MFC and the gelatin matrix, it is thought that the composite failure mechanism might be cohesive within the matrix itself. This is also supported by EDS spectra reported in Supplementary data 3 where low intensity X-ray peaks corresponding to the presence of nitrogen were detected at a dispersive energy of ~0.39 keV. This may indicate the presence of nitrogen atoms at the surface of the MFC after complete sample fracture. The percentage values for nitrogen atoms of 8.9% w/w and 5.4% w/w were obtained respectively for MFC-bovine gelatin and MFC-salmon gelatin nanocomposites. This suggests that some residual gelatin may be present at the MFC surface after complete sample failure, independent of whether bovine or salmon gelatin is used (the molecular structure of cellulose is nitrogen free). Interestingly, the percentage value of nitrogen atoms after sample fracture was higher for MFC that were embedded in bovine gelatin compared to those embedded in salmon gelatin. This result may suggest that a higher amount of residual bovine gelatin might be present at the surface of MFC compared to salmon gelatin. This is consistent with the fact that a stronger interfacial interaction or stress transfer between the surface of MFC and bovine gelatin compared to salmon gelatin was observed from the Raman

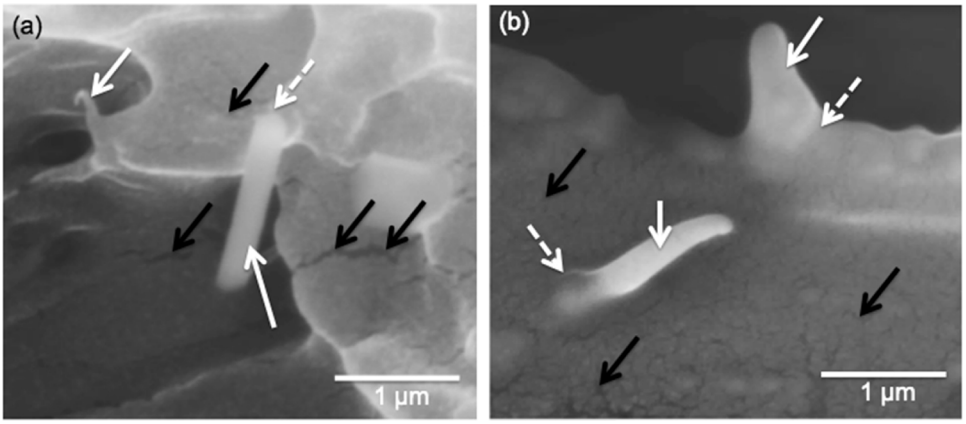

Fig. 9. Typical scanning electron microscopy images obtained from the tensile fracture surface of (a) microfibrillated cellulose-bovine gelatin and (b) microfibrillated cellulose-salmon gelatin nanocomposite films. Black, white and white dotted arrows indicate the presence of cracks occurring within the gelatin matrix, microfibrillated cellulose and the microfibrillated cellulose/gelatin interface respectively.

spectroscopy measurements. Despite the presence of MFC in the gelatin matrix, the brittle nature of gelatin observed at nanoscale cannot be avoided and this may explain why MFC from plant origin have so far been unsuccessful at reinforcing gelatin, especially when using gelatin from mammalian origin and this in addition to the lower stress transfer ability of MFC networks compared to BC networks (Tanpichai et al., 2012).

The mechanical properties of MFC-bovine gelatin and MFC-salmon gelatin nanocomposites, reported in Fig. 8 and Supplementary data 2, can be explained with respect to this cohesive-matrix-fracture mechanism along with the stress transfer quantification. The low mechanical performance of MFC-bovine gelatin nanocomposites compared to MFC-salmon gelatin nanocomposites may be due to a stronger interface between MFC and bovine gelatin compared to salmon gelatin. This strong interface may then be responsible for an early formation of cracks within the bovine gelatin matrix (matrix-cohesive crack formation) compared to the salmon gelatin matrix. If a crack forms and propagates earlier within the bovine gelatin matrix due to a stronger interface, one could expect a low mechanical performance for this composite. On the other hand, a lower stress transfer and better mechanical performance obtained for MFC-salmon gelatin nanocomposite materials compared to MFC-bovine gelatin nanocomposite materials may originate from the formation of a weaker interface between the MFC and salmon gelatin. This weak interface may promote a sufficiently good enough level of interfacial adhesion as well as an interfacial molecular mobility allowing a combination of relatively high Young's modulus, stress and strain at failure, as well as work of fracture. This weaker interface might also induce a delayed crack formation within the salmon gelatin matrix, which might lead to an enhanced mechanical performance. We, however, do not have direct evidence of this is in the present study. It is possible that a better match between the coupling strength exists at the MFC/salmon gelatin interface and the cohesive forces present within the salmon gelatin matrix and MFC compared to the force balance occurring within the MFC-bovine gelatin nanocomposites, which could explain the better mechanical performance of MFC-salmon gelatin nanocomposites compared to MFC-bovine gelatin samples.

4. Conclusions

The interfacial stress transfer between MFC and gelatin was successfully quantified by Raman spectroscopy. This evaluation revealed that stress, is more efficiently transferred from bovine gelatin matrix to the stiffer MFC compared to when a salmon gelatin is used as matrix material. A high stress transfer was, however, not found to be beneficial since the desirable mechanical properties of MFC-salmon gelatin nanocomposites were found to be higher than MFC-bovine gelatin nanocomposites. Higher Young's modulus, stress and strain at failure as well as work of fracture were measured for MFC-salmon gelatin nanocomposites compared to NFC-bovine gelatin nanocomposites at a MFC weight fraction of 15%. The enhanced strength and flexibility measured for MFC-salmon gelatin nanocomposites compared to bovine gelatin-matrix nanocomposites may originate from the different amino acid composition of bovine and salmon gelatin (especially the hydroxyproline amino acid), which may interact differently with the surface of MFC through the formation of a different degree of hydrogen bonding. Another contribution may arise from the higher content in triple-helix configurations in the MFC-salmon gelatin nanocomposites compared to the MFC-bovine gelatin nanocomposites as measured by powder X-ray diffraction. These better mechanical properties obtained for NFC-salmon gelatin nanocomposite films are of interest to the food and the pharmaceutical industries, where they could serve as coatings or encapsulating agents for fresh and minimally processed foods or drugs where good mechanical properties and controlled release are needed. Tensile fracture surface imaging by scanning electron microscopy revealed that fracture within these nanocomposite materials is predominantly occurring within the gelatin matrix rather than at the MFC/gelatin interface or within the MFC itself. This was evidenced by the observation of a high number of nano-sized cracks that form within the gelatin matrix and by the presence of residual gelatin at the MFC surface after sample failure. This was further evidenced by the identification of nitrogen atoms at the surface of MFC by energy dispersive X-ray spectroscopy. Consequently, this study suggests that the mechanical performance and failure of these biomaterials is governed by a cohesive-matrix-failure mechanism and possibly by the coupling and cohesive forces that exist within gelatin, MFC and at the gelatin/MFC interface. This may explain the poor reinforcement ability of MFC from plant origin in gelatin that has been reported so far in the literature.

Conflict of interest

The authors declare that there are no conflicts of interest.

Acknowledgments

F.Q. and J.E. acknowledge financial support from CONICYT/FONDECYT (Nos. 3140036, 1171553) and CONICYT/PCI Newton-Picarte (No. 140144).

Appendix A. Supplementary data

Supplementary data associated with this article can be found, in the online version, at https://doi.org/10.1016/j.carbpol.2018.04.059.

References

Abdul Khalil, H. P. S., Davoudpour, Y., Islam, M. N., Mustapha, A., Sudesh, K., Dungani, R., et al. (2014). Production and modification of nanofibrillated cellulose using

various mechanical processes: A review. *Carbohydrate Polymers, 99*(Supplement C), 649–665.
Arnesen, J. A., & Gildberg, A. (2007). Extraction and characterisation of gelatine from Atlantic salmon (Salmo salar) skin. *Bioresource Technology, 98*(1), 53–57.
Badii, F., MacNaughtan, W., Mitchell, J. R., & Farhat, I. A. (2014). The effect of drying temperature on physical properties of thin gelatin films. *Drying Technology, 32*(1), 30–38.
Benhamou, K., Kaddami, H., Magnin, A., Dufresne, A., & Ahmad, A. (2015). Bio-based polyurethane reinforced with cellulose nanofibers: A comprehensive investigation on the effect of interface. *Carbohydrate Polymers, 122*(Supplement C), 202–211.
Berisio, R., Granata, V., Vitagliano, L., & Zagari, A. (2004). Imino acids and collagen triple helix Stability: Characterization of collagen-like polypeptides containing Hyp-Hyp-Gly sequence repeats. *Journal of the American Chemical Society, 126*(37), 11402–11403.
Besbes, I., Alila, S., & Boufi, S. (2011). Nanofibrillated cellulose from TEMPO-oxidized eucalyptus fibres: Effect of the carboxyl content. *Carbohydrate Polymers, 84*(3), 975–983.
Bigi, A., Panzavolta, S., & Rubini, K. (2004). Relationship between triple-helix content and mechanical properties of gelatin films. *Biomaterials, 25*(25), 5675–5680.
Bulota, M., Tanpichai, S., Hughes, M., & Eichhorn, S. J. (2012). Micromechanics of TEMPO-oxidized fibrillated cellulose composites. *ACS Applied Materials & Interfaces, 4*(1), 331–337.
Chiou, B.-S., Avena-Bustillos, R. J., Shey, J., Yee, E., Bechtel, P. J., Imam, S. H., et al. (2006). Rheological and mechanical properties of cross-linked fish gelatins. *Polymer, 47*(18), 6379–6386.
Díaz, P., López, D., Matiacevich, S., Osorio, F., & Enrione, J. (2011). State diagram of salmon (Salmo salar) gelatin films. *Journal of the Science of Food and Agriculture, 91*(14), 2558–2565.
Díaz-Calderón, P., Flores, E., González-Muñoz, A., Pepczynska, M., Quero, F., & Enrione, J. (2017). Influence of extraction variables on the structure and physical properties of salmon gelatin. *Food Hydrocolloids, 71*(Supplement C), 118–128.
Duan, R., Zhang, J., Liu, L., Cui, W., & Regenstein, J. M. (2018). The functional properties and application of gelatin derived from the skin of channel catfish (Ictalurus punctatus). *Food Chemistry, 239*(Supplement C), 464–469.
Echegaray, M., Mondragon, G., Martin, L., González, A., Peña-Rodriguez, C., & Arbelaiz, A. (2016). Physicochemical and mechanical properties of gelatin reinforced with nanocellulose and montmorillonite. *Journal of Renewable Materials, 4*(3), 206–214.
Fadel, S. M., Hassan, M. L., & Oksman, K. (2012). Improving tensile strength and moisture barrier properties of gelatin using microfibrillated cellulose. *Journal of Composite Materials, 47*(16), 1977–1985.
French, A. D. (2014). Idealized powder diffraction patterns for cellulose polymorphs. *Cellulose, 21*(2), 885–896.
Gómez-Guillén, M. C., Turnay, J., Fernández-Díaz, M. D., Ulmo, N., Lizarbe, M. A., & Montero, P. (2002). Structural and physical properties of gelatin extracted from different marine species: A comparative study. *Food Hydrocolloids, 16*(1), 25–34.
Gómez-Guillén, M. C., Pérez-Mateos, M., Gómez-Estaca, J., López-Caballero, E., Giménez, B., & Montero, P. (2009). Fish gelatin: A renewable material for developing active biodegradable films. *Trends in Food Science & Technology, 20*(1), 3–16.
George, J., & Siddaramaiah (2012). High performance edible nanocomposite films containing bacterial cellulose nanocrystals. *Carbohydrate Polymers, 87*(3), 2031–2037.
Gierlinger, N., Schwanninger, M., Reinecke, A., & Burgert, I. (2006). Molecular changes during tensile deformation of single wood fibers followed by raman microscopy. *Biomacromolecules, 7*(7), 2077–2081.
Gilsenan, P. M., & Ross-Murphy, S. B. (2000). Rheological characterisation of gelatins from mammalian and marine sources. *Food Hydrocolloids, 14*(3), 191–195.
Gudmundsson, M. (2002). Rheological properties of fish gelatins. *Journal of Food Science, 67*(6), 2172–2176.
Harding, S. E. (1997). The intrinsic viscosity of biological macromolecules. Progress in measurement, interpretation and application to structure in dilute solution. *Progress in Biophysics and Molecular Biology, 68*, 207–262.
Haug, I. J., Draget, K. I., & Smidsrød, O. (2004). Physical and rheological properties of fish gelatin compared to mammalian gelatin. *Food Hydrocolloids, 18*(2), 203–213.
Jaipan, P., Nguyen, A., & Narayan, R. J. (2017). Gelatin-based hydrogels for biomedical applications. *MRS Communications, 7*(3), 416–426.
Kargarzadeh, H., Mariano, M., Huang, J., Lin, N., Ahmad, I., Dufresne, A., et al. (2017). Recent developments on nanocellulose reinforced polymer nanocomposites: A review. *Polymer, 132*(Supplement C), 368–393.
Karim, A. A., & Bhat, R. (2008). Gelatin alternatives for the food industry: Recent developments, challenges and prospects. *Trends in Food Science & Technology, 19*(12), 644–656.
Kuijpers, A. J., Engbers, G. H. M., Krijgsveld, J., Zaat, S. A. J., Dankert, J., & Feijen, J. (2000). Cross-linking and characterisation of gelatin matrices for biomedical applications. *Journal of Biomaterials Science, Polymer Edition, 11*(3), 225–243.
Lavoratti, A., Scienza, L. C., & Zattera, A. J. (2016). Dynamic-mechanical and thermo-mechanical properties of cellulose nanofiber/polyester resin composites. *Carbohydrate Polymers, 136*(Supplement C), 955–963.
Lee, K.-Y., Aitomäki, Y., Berglund, L. A., Oksman, K., & Bismarck, A. (2014). On the use of nanocellulose as reinforcement in polymer matrix composites. *Composites Science and Technology, 105*(Supplement C), 15–27.
Liu, Y.-S., Baker, J. O., Zeng, Y., Himmel, M. E., Haas, T., & Ding, S.-Y. (2011). Cellobiohydrolase hydrolyzes crystalline cellulose on hydrophobic faces. *Journal of Biological Chemistry, 286*(13), 11195–11201.
Marquardt, D. (1963). An algorithm for least-squares estimation of nonlinear parameters. *Journal of the Society for Industrial and Applied Mathematics, 11*(2), 431–441.
Matiacevich, S., Celis Cofré, D., Schebor, C., & Enrione, J. (2013). Physicochemical and antimicrobial properties of bovine and salmon gelatin-chitosan films. *CyTA – Journal of Food, 11*(4), 366–378.
Mitchell, J. R., & Ledward, D. A. (1986). *Functional properties of food macromolecules.* Elsevier Applied Science Publishers.
Mondragon, G., Peña-Rodriguez, C., González, A., Eceiza, A., & Arbelaiz, A. (2015). Bionanocomposites based on gelatin matrix and nanocellulose. *European Polymer Journal, 62*(Supplement C), 1–9.
Page, D. H., & El-Hosseiny, F. (1983). The mechanical properties of single wood pulp fibres, part IV. Fibril angle and the shape of the stress-strain curve. *Journal of Pulp and Paper Science, 9*, 99–100.
Park, S., Baker, J. O., Himmel, M. E., Parilla, P. A., & Johnson, D. K. (2010). Cellulose crystallinity index: Measurement techniques and their impact on interpreting cellulase performance. *Biotechnology for Biofuels, 3*(1), 10.
Pei, Y., Yang, J., Liu, P., Xu, M., Zhang, X., & Zhang, L. (2013). Fabrication, properties and bioapplications of cellulose/collagen hydrolysate composite films. *Carbohydrate Polymers, 92*(2), 1752–1760.
Piez, K. A., & Gross, J. (1960). The amino acid composition of some fish collagens: The relation between composition and structure. *Journal of Biological Chemistry, 235*(4), 995–998.
Poyraz, B., Tozluoğlu, A., Candan, Z., Demir, A., Yavuz, M., Büyuksarı, Ü., et al. (2018). TEMPO-treated CNF composites: Pulp and matrix effect. *Fibers and Polymers, 19*(1), 195–204.
Poyraz, B., Tozluoğlu, A., Candan, Z., & Demir, A. (2017). Matrix impact on the mechanical, thermal and electrical properties of microfluidized nanofibrillated cellulose composites. *Journal of Polymer Engineering, 37*, 921.
Poyraz, B., Tozluoğlu, A., Candan, Z., Demir, A., & Yavuz, M. (2017). Influence of PVA and silica on chemical, thermo-mechanical and electrical properties of celluclast-treated nanofibrillated cellulose composites. *International Journal of Biological Macromolecules, 104*, 384–392.
Qing, Y., Sabo, R., Zhu, J. Y., Agarwal, U., Cai, Z., & Wu, Y. (2013). A comparative study of cellulose nanofibrils disintegrated via multiple processing approaches. *Carbohydrate Polymers, 97*(1), 226–234.
Quero, F., Nogi, M., Yano, H., Abdulsalami, K., Holmes, S. M., Sakakini, B. H., et al. (2010). Optimization of the mechanical performance of bacterial cellulose/Poly(l-lactic) acid composites. *ACS Applied Materials & Interfaces, 2*(1), 321–330.
Quero, F., Eichhorn, S. J., Nogi, M., Yano, H., Lee, K.-Y., & Bismarck, A. (2012). Interfaces in cross-linked and grafted bacterial cellulose/poly(lactic acid) resin composites. *Journal of Polymers and the Environment, 20*(4), 916–925.
Quero, F., Coveney, A., Lewandowska, A. E., Richardson, R. M., Díaz-Calderón, P., Lee, K.-Y., et al. (2015). Stress transfer quantification in gelatin-matrix natural composites with tunable optical properties. *Biomacromolecules, 16*(6), 1784–1793.
Rebane, R., & Herodes, K. (2010). A sensitive method for free amino acids analysis by liquid chromatography with ultraviolet and mass spectrometric detection using precolumn derivatization with diethyl ethoxymethylenemalonate: Application to the honey analysis. *Analytica Chimica Acta, 672*(1), 79–84.
Rusli, R., & Eichhorn, S. J. (2008). Determination of the stiffness of cellulose nanowhiskers and the fiber-matrix interface in a nanocomposite using Raman spectroscopy. *Applied Physics Letters, 93*(3), 033111.
Rusli, R., Shanmuganathan, K., Rowan, S. J., Weder, C., & Eichhorn, S. J. (2010). Stress-transfer in anisotropic and environmentally adaptive cellulose whisker nanocomposites. *Biomacromolecules, 11*(3), 762–768.
Saito, T., Kuramae, R., Wohlert, J., Berglund, L. A., & Isogai, A. (2013). An ultrastrong nanofibrillar biomaterial: The strength of single cellulose nanofibrils revealed via sonication-Induced fragmentation. *Biomacromolecules, 14*(1), 248–253.
Sarwar, M. S., Niazi, M. B. K., Jahan, Z., Ahmad, T., & Hussain, A. (2018). Preparation and characterization of PVA/nanocellulose/Ag nanocomposite films for antimicrobial food packaging. *Carbohydrate Polymers, 184*, 453–464.
Schrieber, R. (2007). *Gelatine handbook: Theory and industrial practice.* Weinheim: Wiley-VCH2007 Chichester: John Wiley [distributor], 2007.
Segal, L., Creely, J. J., Martin, A. E., & Conrad, C. M. (1959). An empirical method for estimating the degree of crystallinity of native cellulose using the X-ray diffractometer. *Textile Research Journal, 29*(10), 786–794.
Sinthusamran, S., Benjakul, S., & Kishimura, H. (2015). Molecular characteristics and properties of gelatin from skin of seabass with different sizes. *International Journal of Biological Macromolecules, 73*(Supplement C), 146–153.
Tanpichai, S., Quero, F., Nogi, M., Yano, H., Young, R. J., Lindström, T., et al. (2012). Effective young's modulus of bacterial and microfibrillated cellulose fibrils in fibrous networks. *Biomacromolecules, 13*(5), 1340–1349.
Tanpichai, S., Sampson, W. W., & Eichhorn, S. J. (2014). Stress transfer in microfibrillated cellulose reinforced poly(vinyl alcohol) composites. *Composites Part A: Applied Science and Manufacturing, 65*(Supplement C), 186–191.
Tonoli, G. H. D., Teixeira, E. M., Corrêa, A. C., Marconcini, J. M., Caixeta, L. A., Pereira-da-Silva, M. A., et al. (2012). Cellulose micro/nanofibres from Eucalyptus kraft pulp: Preparation and properties. *Carbohydrate Polymers, 89*(1), 80–88.
Tozluoğlu, A., Poyraz, B., Candan, Z., Yavuz, M., & Arslan, R. (2017). Biofilms from micro/nanocellulose of NaBH4-modified kraft pulp. *Bulletin of Materials Science, 40*(4), 699–710.
Veis, A. (1964). *The macromolecular chemistry of gelatin.* New York: Academic Press.
Wiley, J. H., & Atalla, R. H. (1987). Band assignments in the Raman spectra of celluloses. *Carbohydrate Research, 160*(Supplement C), 113–129.
Yakimets, I., Wellner, N., Smith, A. C., Wilson, R. H., Farhat, I., & Mitchell, J. (2005). Mechanical properties with respect to water content of gelatin films in glassy state. *Polymer, 46*(26), 12577–12585.
Zhang, Z., Li, G.-Y., & Shi, B. L. (2006). Physicochemical properties of collagen, gelatin and collagen hydrolysate derived from bovine limed split wastes. *Journal of the Society of Leather Technologists and Chemists, 90*(1), 23–28.